Nanoimpact Electrochemistry to Quantify the Transformation and Electrocatalytic Activity of Ni(OH)$_2$ Nanoparticles: Toward Size-activity Relationship at High Throughput

Mathias Miranda Vieira, Jean-François Lemineur, Jérôme Médard, Catherine Combellas, Frédéric Kanoufi, Jean-Marc Noël*

Université Paris Cité, ITODYS, CNRS, F-75013 Paris, France.

AUTHOR INFORMATION

Corresponding Author

* jean-marc.noel@u-paris.fr

ABSTRACT

The fast establishment of structure-reactivity relationships is crucial to identify the most appropriate nanoparticles (NPs) for a given application. This requires the development of methodologies allowing, simultaneously, to unravel the NPs geometry and screen their reactivity. Herein nanoimpact electrochemistry (NIE) allows quantifying the transformation and measuring the electrocatalytic activity for the oxygen evolution reaction (OER) of >100 Ni(OH)$_2$ NPs of a wide range of size (NP radii from 25 to 100nm). This is achieved by scanning electrochemical microscopy in a generation/collection like mode, one electrode being used to electro-generate by local precipitation colloidal Ni(OH)$_2$ NPs and the second one to collect them by NIE. It allows i)

quantifying the reductive and oxidative conversion of the $Ni(OH)_2$ NPs and, ii) separating the electrochemical conversion and the OER electrocatalysis, leading to the evaluation of a structure-activity relationship.

TOC GRAPHICS
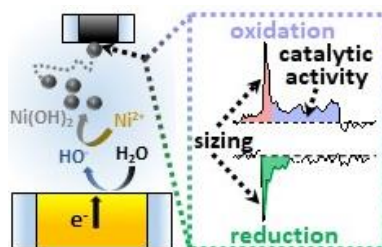
KEYWORDS Scanning electrochemical microscopy, single entity electrochemistry, electrosynthesis, electrocatalysis, insertion/disinsertion.

Transition metal oxides and hydroxides are promising abundant materials for energy conversion and storage.[1–3] In the context of electrocatalytic reactions including the oxygen evolution reaction (OER),[4–6] and ion insertion[7–10], nickel hydroxides present interesting physicochemical properties that can be optimized when the material is nanostructured.[11] Since those properties are closely linked to the composition, size and morphology of the nanoscale objects, methodologies allowing fast establishment of structure-activity relationships are essential to identify the most appropriate nanomaterial for a given application.

Single entity nanoimpact electrochemistry (NIE) has emerged as an easily implementable analytical technique to study at high throughput the reactivity of single nano-objects in solution, such as nanoparticles (NPs).[12–17] The analysis of the current spikes (shape, and amplitude) arising from the collisions of individual NPs with a biased ultramicroelectrode (UME) allows extracting information about the colloidal system under investigation including nickel based NPs.[18–20] Generally, NIE experiments are carried out at an UME plunging in a large volume of diluted colloidal NPs. This allowed discriminating different NPs populations,[21] deciphering mechanisms of NPs transformation,[13,22] quantifying electrocatalytic reaction rates[19,23–26] or physicochemical processes such as NPs-substrate[21,27] or NPs-electrolyte[28] interactions. However, NIE remains rarely employed to establish structure-activity relationships (except *i.e.* anodic−cathodic nano-collisions at fast pulse potentials[29] and correlative methods combined with optical microscopies[30–33]). Herein, we propose a new NIE approach allowing to i) quantify at high throughput the conversion of electrosynthesized $Ni(OH)_2$ NPs and, ii) discriminate the electrochemical conversion of the NPs and their reactivity against OER, leading to a fast establishment of size-activity relationships. This is performed in an electrochemical generation/collection mode of scanning electrochemical microscopy (SECM).[34] This configuration, already employed to investigate NPs transformation[35] or dissolution,[36] uses one electrode to electrogenerate colloidal $Ni(OH)_2$ NPs from solution of Ni salts whereas a second one collects and probes their activity by NIE during their formation (Figures 1a and SI1). This offers several advantages: (i) the generating electrode allows on demand production of NPs with tuned concentration and size;[37] particularly a wide distribution of size is possible enabling to explore size-activity relationships and, (ii) the collecting microelectrode allows a non-destructive probing of the NPs at high

throughput since, thanks to their transport, only a limited but statistically relevant population of the NPs is titrated by NIE.[35]
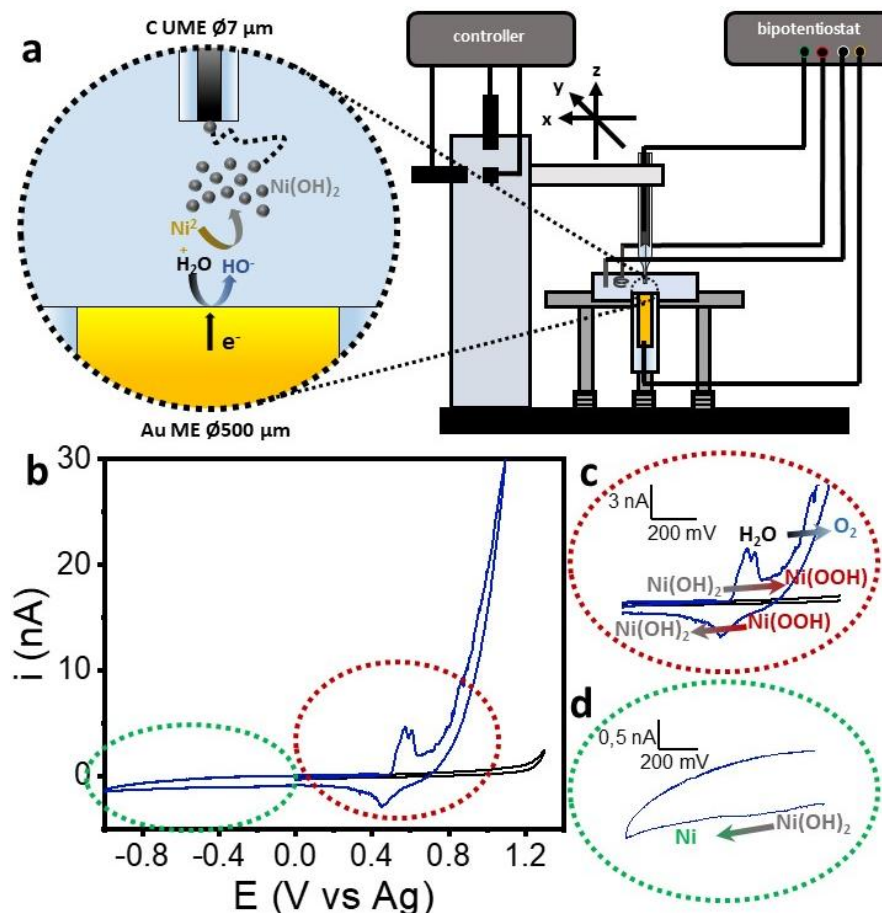

Figure 1. (a) NIE-SECM configuration to investigate the transformation and reactivity of Ni(OH)$_2$ NPs during their electrosynthesis. (b) CVs at a C-UME held at 25μm from an Au-ME in aqueous solution containing 0.1M KCl, 5mM NiCl$_2$ and 10mM citrate, before (black) and after (blue) polarizing the Au-ME at E_{Au}=-1.3V vs Ag-QRE. v=50mV.s^{-1}. (c) and (d): Zoom in the anodic and cathodic parts of the CVs, respectively

Microscopic evidence of Ni(OH)$_2$ formation. Details can be found in Sections 2 and 3 in SI. The NIE-SECM configuration uses a 500μm diameter gold microelectrode (Au-ME) generator to increase locally the pH of a solution containing 0.1M KCl, 5mM NiCl$_2$ and 10mM citrate by

4

applying a potential to reduce H_2O (Equation (1)) and produce colloidal $Ni(OH)_2$ NPs in the diffusion layer of the Au-ME (Equation (2)).

$$4H_2O + 4e^- \rightarrow 4HO^- + 2H_2 \qquad (1)$$

$$2HO^- + Ni^{2+} \rightarrow Ni(OH)_2 \qquad (2)$$

The collector is a 7µm carbon fiber ultramicroelectrode (C-UME) facing the Au-ME; it probes in its reaction layer the transformation of the NPs.

The formation of $Ni(OH)_2$ was first demonstrated by cyclic voltammetry (CV) at the C-UME held at 25µm from the Au-ME in the Ni^{2+} solution (Figure 1b). While the CV displays no Faradic current before applying any potential to the Au-ME, (Figure 1b, black), right after application of a constant potential, E_{Au}=-1.3V vs Ag-QRE for 100s (Figure 1b and c, blue), the CV shows a quasi reversible redox process centred at $E^{0'} \approx 0.5$ V vs Ag-QRE. The corresponding oxidation and reduction peaks are characteristic of the oxidation of $Ni(OH)_2$ to $Ni(OOH)$ and of the reverse reduction, respectively (Equation (3)).[38–41]

$$Ni(OH)_2 \rightleftharpoons Ni(OOH) + H^+ + e^- \qquad (3)$$
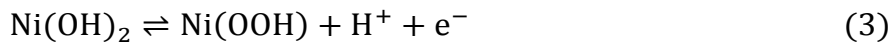
This oxidation is followed by another one at more anodic potential that is attributed to OER (Equation (4)) known to be catalysed by $Ni(OOH)$ in alkaline media.[38–41] A rather weak and not well-defined reduction peak is present between -0.3 and -0.9V that can be associated to the reduction of $Ni(OH)_2$ to metallic Ni (Figure 1d, Equation (5)).[42] The

poor detection of this peak may be related to the partial reduction of $Ni(OH)_2$ thin films when probed by CV at scan rates > $0.2mV.s^{-1}$.[42]

$$2H_2O \rightarrow O_2 + 4H^+ + 4e^- \qquad (4)$$

$$Ni(OH)_2 + 2e^- \rightarrow Ni + 2HO^- \qquad (5)$$
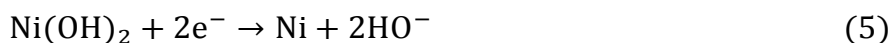
This experiment attests the presence of $Ni(OH)_2$ on the C-UME resulting from the formation of $Ni(OH)_2$ within the diffusion layer of the Au-ME. Moreover, "noisy" stochastic current spikes on the CV suggest the presence of free NPs colliding stochastically the C-UME.[43]

$Ni(OH)_2$ NPs characterization by reductive nanoimpacts. The formation of $Ni(OH)_2$ NPs was characterized *in situ* by reductive NIE. Chronoamperograms were recorded at a C-UME polarized at E_C=-0.6V vs Ag-QRE for 120s, while the Au-ME was polarized at E_{Au}=-1.3V vs Ag-QRE (Figure SI2a). The current at the C-UME (Figures 2a and SI2a) reveals reduction current spikes immediately after ca. 0.8s (Figure SI2a). These spikes showing a sharp rise of absolute current followed by a slower return to baseline (inset of Figure 2a) are characteristic of NPs transformation,[44] here attributed to the reduction of individual $Ni(OH)_2$ NPs to Ni NPs (Equation (5), sketched in Figure 2b). The reduction spikes last for few tens of milliseconds (see nanoimpacts inset of Figure 2a and histogram of Figure SI2b). This rapid reduction at the scale of individual NPs is in contrast to the slow reduction during CV for adsorbed $Ni(OH)_2$.[42] The enhanced activity of colloids during electrochemical collisions compared to adsorbed ones has been already

highlighted.[25,33] The charge, Q_{red}, associated to each current spike (inset of Figure 2c), allowed estimating an apparent size of the electrochemically reduced $Ni(OH)_2$ NPs, defined as an equivalent NP radius, $r_{EC,red}$ (Equation (6)):

$$r_{EC,red} = \sqrt[3]{\frac{3Q_{red}M}{4\pi zF\rho}} \qquad (6)$$

with M and ρ the molar mass and density of $Ni(OH)_2$, F the Faraday constant and z the number of electron exchanged.
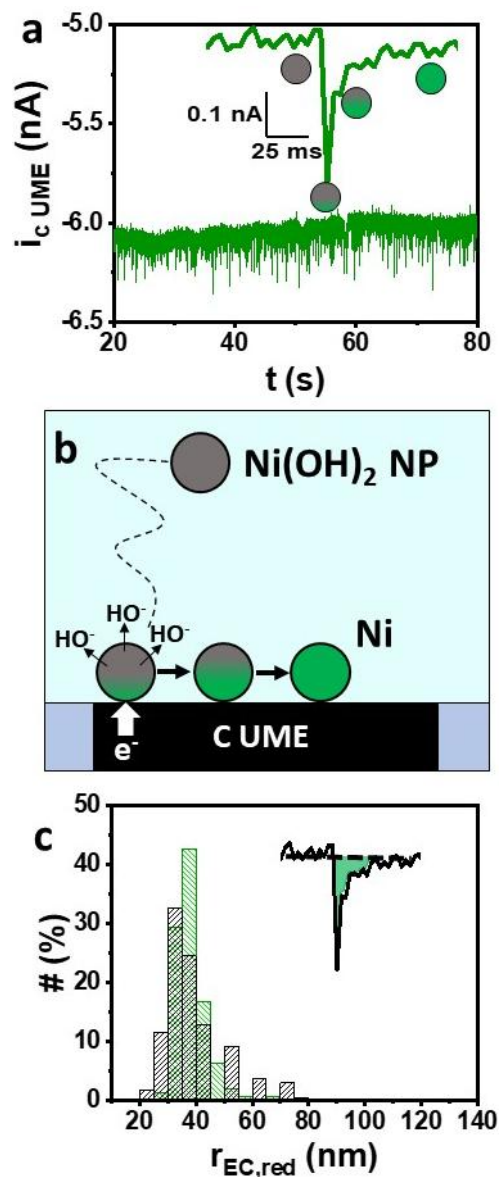
Figure 2. Ni(OH)$_2$ NPs characterization by reductive NIE. (a) Chronoamperogram at the C-UME biased at E_C=-0.6 V vs Ag-QRE, held at 25μm from the Au-ME polarized at E_{Au}=-1.2V vs Ag-QRE. Inset: zoom of one spike. (b) Mechanism of the reduction of Ni(OH)$_2$ NPs to Ni. (c) Size distribution obtained from the nanoimpacts (green) and from the SEM images (black). Inset: example of the charge considered to evaluate the size of one NP.

The radius distribution is centred at $r_{EC,red}$=37±7nm (Figure 2c, green), in good agreement with the one obtained by SEM (black histogram in Figure 2c) suggesting a complete

electrochemical reduction of the $Ni(OH)_2$ NPs. SEM reveals spherical-like NPs attributed to $Ni(OH)_2$ NPs (Figure SI3a). The good agreements between both distributions coupled to the long time period observed between each collision event (>100ms for >90% of NPs) suggests that one collision corresponds to one NP rather than multiple collisions of one single NPs.[33,45–48]

$Ni(OH)_2$ NPs characterization by oxidative nanoimpacts. In another set of experiments, the C-UME, placed at 50µm from the Au ME, was biased at E_C=+1V vs Ag-QRE. The current transient at the C-UME (Figure 3a) reveals oxidation spikes. Their shape is significantly different from that of the reductive ones since the peak-shaped transient is immediately followed by a current step before return to baseline (inset of Figure 3a). A fast EC response followed by slow activity was interpreted as a consequence of NP-electrode interaction for Ag NPs oxidative dissolution.[21] However, here, the EC charge of the current transient leads to a large electrochemical overestimation of the NP size ($r_{EC,ox}$=105±34nm, see Figure 3b) compared to the geometrical size distribution established from SEM images ($r_{SEM,ox}$=71±20nm, see Figure SI4) considering a one-electron oxidative full conversion of $Ni(OH)_2$ into $Ni(OOH)$.[38–41] Noteworthy, the highest size distribution recorded under this experimental condition is expected as the NPs size should increase with the distance between both electrodes.[35] It demonstrates the potentiality of such configuration to probe the reactivity of a wide distribution of NPs sizes.

The discrepancy between the distribution observed by NIE and SEM reveals that the electrochemical transient contains not only the contribution of the EC conversion of

Ni(OH)$_2$ into NiOOH, but also another contribution. The current step following the current spike is typical of electrocatalytic NIE,[24,49,50] and is attributed to the newly formed NiOOH NPs that drive the electrocatalysis of water oxidation (Figure 3c). Indeed at the 1V vs Ag-QRE electrode polarization, both Ni(OH)$_2$ oxidation and electrocatalysis of OER by the resulting NiOOH NPs can occur (Figure 1b). Additionally, looking precisely to the current spikes for some of them (~10%), multi steps within ~50ms can be visualized for which the current spike always appears at the first step and is followed by discontinued current steps (Figure SI5). This allows distinguishing multiple collision events of individual Ni(OH)$_2$ NPs for which the first step corresponds to their oxidation followed by their catalytic activity.
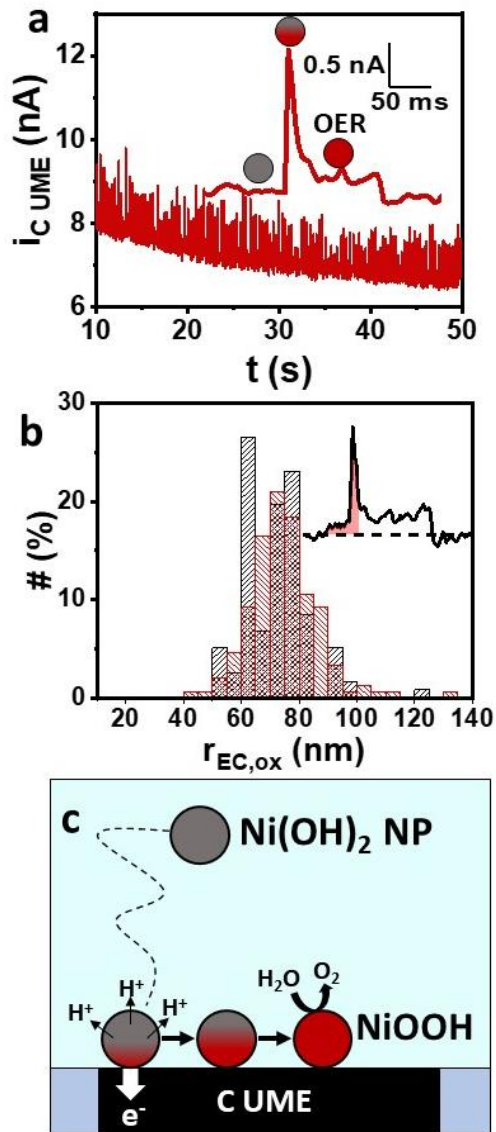
Figure 3. Ni(OH)$_2$ NPs characterization by oxidative nanoimpacts. (a) Chronoamperogram at the C-UME biased at E_C=1V vs Ag-QRE, held at 50μm from the Au-ME polarized at E_{Au}=-1.2V vs Ag-QRE. Inset: zoom of one spike. (b) Histogram showing the size distribution obtained from nanoimpacts (red) and from SEM images (black). Inset: example of the charge considered to evaluate the size of one NP. (c) Mechanism proposed for Ni(OH)$_2$ NPs oxidation followed by OER.

Even if both contributions are somehow interrelated, a first simplification was made by assuming that the fast current spike corresponds to $Ni(OH)_2$ conversion into NiOOH while the longer current step corresponds to electrocatalysis. The NPs sizes was estimated by considering only the charge Q_{ox} under the current spike (red part in inset of Figure 3b), which gives an electrochemical NP radius distribution, $r_{EC,ox}$=74±18nm in excellent agreement with that obtained by SEM (Figure 3b).

Therefore, the current steps were interpreted as the electrocatalysis of OER by NiOOH NPs (Figures 4a and SI6a, purple area). Such electrocatalysis was analyzed for different NP sizes ($r_{EC,ox}$ extracted from Q_{ox}). For N=140 EC spikes, the electrocatalytic activity lasts for 80±5ms and is independent of the NPs size (Figure SI6c). It ends by an abrupt current drop, in line with the reported OER activity on $CoFe_2O_4$ NPs,[24] likely due to a rapid electrical disconnection of the NP rather than its progressive deactivation due to O_2 gas accumulation around the NP. Indeed, similarly to what has been observed,[24] there is no correlation between the amount of O_2 produced (charge of the current step, Q_{cat}) and the size of the NPs (Figure SI6c).

Structure-activity relationship of $Ni(OH)_2$ conversion and electrocatalysis. Firstly, the dynamics of the NP conversion was analysed for the oxidative and reductive processes. In both cases the amplitude and duration of the nanoimpact current spikes increase with the NPs radius, r_{EC} (Figure SI7a,b and SI7c,d, respectively). Noteworthy, the reduction of $Ni(OH)_2$ at more reductive potential (-0.8V) reveals chronoamperogram (Figure SI8a) and distribution of nanoimpact charge, current amplitude and duration similar to those at -0.6V (Figure SI8b). It indicates that the reduction process is limited by

mass transfer rather than by electrochemical kinetics. Owing to the relatively large NP size (>50nm), a limitation by the solid-state diffusion of HO$^-$ is expected within the NP during its transformation (inset of Figure 4b, green). Assuming that the size variation of the NP is not significantly altered during the conversion (<15% NP size variation expected from Ni(OH)$_2$ to Ni(OOH) [51]), the peak duration, Δt, should be related to the initial NP radius, r_0, (Equation (8)):[52]

$$\Delta t = \frac{r_0^2}{3 V_M^{Ni(OH)_2} D_{HO^-} C_{max}} \tag{8}$$

with D the diffusion coefficient of HO$^-$ within the Ni(OH)$_2$ NP and C_{max} its maximum concentration (mol.cm^{-3})$\approx 2/V_M^{Ni(OH)_2}$ in the Ni(OH)$_2$ NP. This yields $r_0^2 \approx 6 D_{HO^-} \Delta t$.
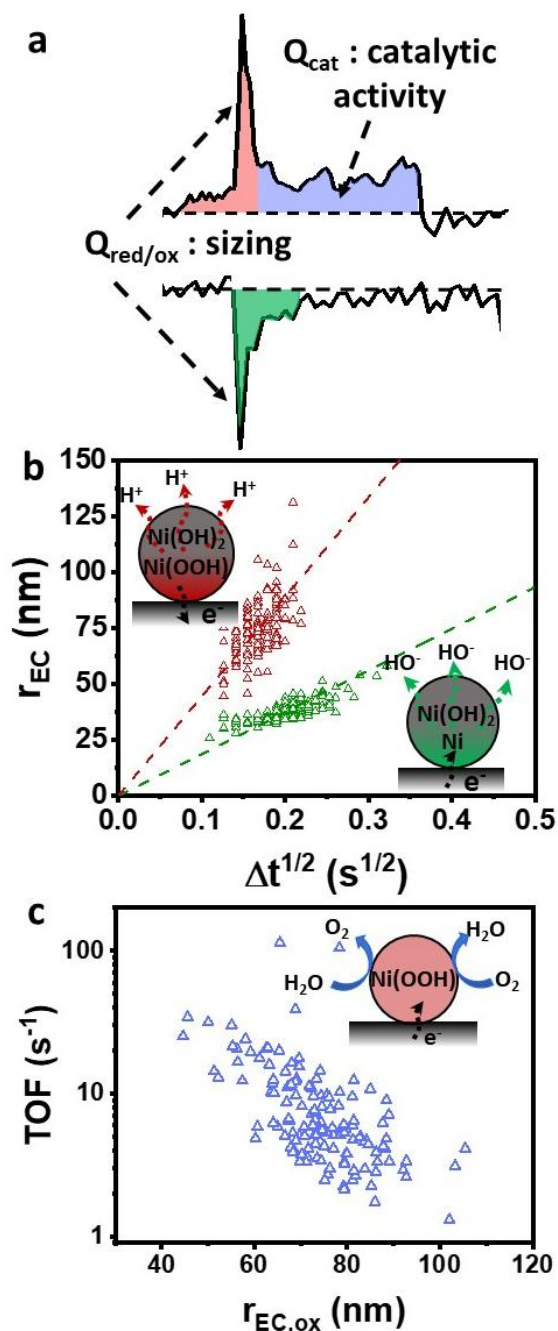
Figure 4: (a) Analysis of an individual current signal for oxidative and reductive nanoimpacts. (b) NP radius vs the square root of peak duration for $E_{C\ UME}$=-0.6 V (green) and +1V (red). Dotted lines: linear fits to determine the diffusion coefficients of HO^- (green) and H^+ (red) within the NPs using Equation (8). (c) Turnover frequency (TOF) of individual NPs as a function of their electrochemical radius $r_{EC,ox}$.

r_{EC}, evaluated at -0,6V evolves linearly with the square root of the peak duration (Figure 4b, green), confirming a diffusional limitation. The same relationship is found at -0.8V (Figure SI8e). By fitting the scatterplots by Equation (8), the diffusion coefficient of HO⁻ ions in Ni(OH)$_2$ NPs during their reduction is $D_{HO-}\approx6\times10^{-11}$ cm^2.s^{-1}, a value within the range of solid phase ion diffusion.

The same analysis for the oxidation of Ni(OH)$_2$ NPs (Figure 4b, red) evidences similar linear relationship with a higher slope. The limiting process is then the disinsertion of H$^+$ within the NPs (inset of Figure 4b). By fitting the data with Equation (8) and considering the maximum H$^+$ concentration that can be removed from the structure, $C_{max,H+}$ (mol.cm^{-3})$\approx1/V_M^{Ni(OH)_2}$, the diffusion coefficient of H$^+$ is $D_{H+}\approx5\times10^{-10}$cm².s^{-1}, a value within the range of those already reported.[41,53] D_{H+} is one order of magnitude faster than D_{HO-} extracted from the analysis of the reduction spike, which is attributed to the lower sterically hindrance of H$^+$ compared to HO⁻. This involves a faster disinsertion process for oxidation of Ni(OH)$_2$ than for reduction.

Secondly, the catalytic charge, Q_{cat}, exchanged during the current step was measured for each nanoimpact. From Q_{cat}, a turnover frequency, *TOF*, was evaluated providing the catalytic activity for OER at the single NP level using equation (9), (Section 3 in SI):

$$TOF = \frac{Q_{cat}}{4Q_{ox}\Delta t_{cat}} \qquad (9)$$

with Q_{ox} the charge for the oxidative spike for each nanoimpact, (see Figure 4a) and Δt_{cat} the duration of the current step attributed to the catalytic process. This assumes that the entire volume of the NP is involved in the OER electrocatalysis, allowing a comparison with the previous work performed on individual $Ni(OH)_2$ NPs immobilized on a nanoelectrode.[41] The *TOF* values decrease with the NP radii (Figure 4c) and are of the same order of magnitude as those previously reported for single NPs electrodeposited on a nanoelectrode.[41]

To summarize SECM was used in a generation/collection configuration to simultaneously electrosynthesize $Ni(OH)_2$ NPs (NPs radii ranging from 25 to 100nm) and investigate their electrochemical conversion and reactivity during their formation. Such SECM-NIE strategy allows analyzing the reductive transformation of $Ni(OH)_2$ NPs into metallic Ni and their oxidative conversion into NiOOH NPs. Both conversions are controlled by HO^- or H^+ ions transport within the NPs. The faster NPs oxidative conversion compared to the reductive one suggests a ~10 times faster diffusion coefficient of H^+ with respect to HO^- in the Ni-based solid oxide. The oxidative nanoimpact transients carry more electrochemical information. Indeed, a ca. 100 ms longer current tail provides valuable information on the electrocatalysis of OER by NiOOH NPs, as confirmed by the *TOF* values that decrease when increasing the NP size in agreement with previous study for $Ni(OH)_2$ NPs immobilized on nanoelectrodes.[41] The separation of electrochemical conversion and electrocatalysis allowed, for the first time, determining size-reactivity relationships. Both the simple electrosynthetic approach and the complete characterization of the NPs in the NIE-SECM configuration could be extended to other

types of oxides NPs, implementable in microfluidic platforms. Besides, the double process characterization, here exemplified for OER, opens new ways toward the determination of structure-activity relationships at high throughput for other NPs involved in anodic or cathodic electrocatalysis.

ASSOCIATED CONTENT

Supporting Information

The Supporting Information is available free of charge at XXX.

Material and methods (electrosynthetic procedure, SEM, electrochemical experiments, SEM), dark field optical microscopy experiments, characterization of the NPs by nanoimpacts and determination of the turn over frequency.

AUTHOR INFORMATION

Corresponding author

Jean-Marc Noel - Université Paris Cité, ITODYS, CNRS, F-75013 Paris, France.

orcid.org/0000-0001-8278-7748

Email: jean-marc.noel@cnrs.fr

Authors

Mathias Miranda Vieira - Université Paris Cité, ITODYS, CNRS, F-75013 Paris, France.

Jean-François Lemineur - Université Paris Cité, ITODYS, CNRS, F-75013 Paris, France.

Jérôme Médard - Université Paris Cité, ITODYS, CNRS, F-75013 Paris, France.

Catherine Combellas - Université Paris Cité, ITODYS, CNRS, F-75013 Paris, France.

Frédéric Kanoufi - Université Paris Cité, ITODYS, CNRS, F-75013 Paris, France.

0000-0002-9784-2380

Notes

The authors declare no competing financial interests.

REFERENCES

(1)   McCrory, C. C. L.; Jung, S.; Peters, J. C.; Jaramillo, T. F. Benchmarking Heterogeneous Electrocatalysts for the Oxygen Evolution Reaction. *J. Am. Chem. Soc.*, **2013**, *135*, 16977–16987.

(2)   Trotochaud, L.; Ranney, J. K.; Williams, K. N.; Boettcher, S. W. Solution-Cast Metal Oxide Thin Film Electrocatalysts for Oxygen Evolution. *J. Am. Chem. Soc.*, **2012**, *134*, 17253–17261.

(3)   Fan, G.; Li, F.; Evans, D. G.; Duan, X. Catalytic Applications of Layered Double Hydroxides: Recent Advances and Perspectives. *Chem. Soc. Rev.*, **2014**, *43*, 7040–7066.

(4)   Luan, C.; Liu, G.; Liu, Y.; Yu, L.; Wang, Y.; Xiao, Y.; Qiao, H.; Dai, X.; Zhang, X. Structure Effects of 2D Materials on α-Nickel Hydroxide for Oxygen Evolution Reaction. *ACS Nano*, **2018**, *12*, 3875–3885.

(5)   Chen, Y.; Rui, K.; Zhu, J.; Dou, S. X.; Sun, W. Recent Progress on Nickel-Based Oxide/(Oxy)Hydroxide Electrocatalysts for the Oxygen Evolution Reaction. *Chem. Eur.*

J., **2019**, *25*, 703–713.

(6)   Sharel, P. E.; Liu, D.; Lazenby, R. A.; Sloan, J.; Vidotti, M.; Unwin, P. R.; Macpherson, J. V. Electrodeposition of Nickel Hydroxide Nanoparticles on Carbon Nanotube Electrodes: Correlation of Particle Crystallography with Electrocatalytic Properties. *J. Phys. Chem. C*, **2016**, *120*, 16059–16068.

(7)   Han, X. J.; Xu, P.; Xu, C. Q.; Zhao, L.; Mo, Z. B.; Liu, T. Study of the Effects of Nanometer β-Ni(OH)2 in Nickel Hydroxide Electrodes. *Electrochim. Acta*, **2005**, *50*, 2763–2769.

(8)   Kiani, M. A.; Mousavi, M. F.; Ghasemi, S. Size Effect Investigation on Battery Performance: Comparison between Micro- and Nano-Particles of β-Ni(OH)2 as Nickel Battery Cathode Material. *J. Power Sources*, **2010**, *195*, 5794–5800.

(9)   Xiong, X.; Ding, D.; Chen, D.; Waller, G.; Bu, Y.; Wang, Z.; Liu, M. Three-Dimensional Ultrathin Ni(OH)2 Nanosheets Grown on Nickel Foam for High-Performance Supercapacitors. *Nano Energy*, **2015**, *11*, 154–161.

(10)   Ji, J.; Zhang, L. L.; Ji, H.; Li, Y.; Zhao, X.; Bai, X.; Fan, X.; Zhang, F.; Ruoff, R. S. Nanoporous Ni(OH)2 Thin Film on 3d Ultrathin-Graphite Foam for Asymmetric Supercapacitor. *ACS Nano*, **2013**, *7*, 6237–6243.

(11)   Kleijn, S. E. F.; Lai, S. C. S.; Koper, M. T. M.; Unwin, P. R. Electrochemistry of Nanoparticles. *Angew. Chem. Int. Ed.*, **2014**, *53*, 3558–3586.

(12)   Peng, Y. Y.; Qian, R. C.; Hafez, M. E.; Long, Y. T. Stochastic Collision Nanoelectrochemistry: A Review of Recent Developments. *ChemElectroChem*, **2017**, *4*, 977–985.

(13)   Defnet, P. A.; Anderson, T. J.; Zhang, B. Stochastic Collision Electrochemistry of Single Silver Nanoparticles. *Curr. Opin. Electrochem.*, **2020**, *22*, 129–135.

(14)   Stevenson, K. J.; Tschulik, K. A Materials Driven Approach for Understanding Single Entity Nano Impact Electrochemistry. *Curr. Opin. Electrochem.*, **2017**, *6*, 38–45.

(15)   Peng, Y. Y.; Guo, D.; Ma, W.; Long, Y. T. Intrinsic Electrocatalytic Activity of Gold Nanoparticles Measured by Single Entity Electrochemistry. *ChemElectroChem*, **2018**, *5*, 2982–2985.

(16)   Patrice, F. T.; Qiu, K.; Ying, Y. L.; Long, Y. T. Single Nanoparticle Electrochemistry. *Annu. Rev. Anal. Chem.*, **2019**, *12*, 347–370.

(17)   Lu, S. M.; Chen, J. F.; Peng, Y. Y.; Ma, W.; Ma, H.; Wang, H. F.; Hu, P.; Long, Y. T. Understanding the Dynamic Potential Distribution at the Electrode Interface by Stochastic Collision Electrochemistry. *J. Am. Chem. Soc.*, **2021**, *143*, 12428–12432.

(18)   Stuart, E. J. E.; Zhou, Y. G.; Rees, N. V.; Compton, R. G. Determining Unknown Concentrations of Nanoparticles: The Particle-Impact Electrochemistry of Nickel and Silver. *RSC Adv.*, **2012**, *2*, 6879–6884.

(19)   Zhou, Y. G.; Rees, N. V.; Compton, R. G. Electrochemistry of Nickel Nanoparticles Is Controlled by Surface Oxide Layers. *Phys. Chem. Chem. Phys.*, **2013**, *15*, 761–763.

(20)   Zhou, Y. G.; Haddou, B.; Rees, N. V.; Compton, R. G. The Charge Transfer Kinetics of the Oxidation of Silver and Nickel Nanoparticles via Particle-Electrode Impact Electrochemistry. *Phys. Chem. Chem. Phys.*, **2012**, *14*, 14354–14357.

(21)   Ma, H.; Chen, J.-F.; Wang, H.-F.; Hu, P.-J.; Ma, W.; Long, Y.-T. Exploring Dynamic Interactions of Single Nanoparticles at Interfaces for Surface-Confined Electrochemical Behavior and Size Measurement. *Nat. Commun.*, **2020**, *11*, 2307.

(22)   Saw, E. N.; Kratz, M.; Tschulik, K. Time-Resolved Impact Electrochemistry for Quantitative Measurement of Single-Nanoparticle Reaction Kinetics. *Nano Res.*, **2017**, *10*, 3680–3689.

(23)   Xiao, Y.; Fan, F. R. F.; Zhou, J.; Bard, A. J. Current Transients in Single Nanoparticle Collision Events. *J. Am. Chem. Soc.*, **2008**, *130*, 16669–16677.

(24)   El Arrassi, A.; Liu, Z.; Evers, M. V.; Blanc, N.; Bendt, G.; Saddeler, S.; Tetzlaff, D.; Pohl, D.; Damm, C.; Schulz, S. et al. Intrinsic Activity of Oxygen Evolution Catalysts Probed at

Single CoFe2O4 Nanoparticles. *J. Am. Chem. Soc.*, **2019**, *141*, 9197–9201.

(25)   Chen, M.; Lu, S.-M.; Peng, Y.-Y.; Ding, Z.; Long, Y.-T. Tracking Electrocatalytic Activity of a Single Palladium Nanoparticle for Hydrogen Evolution Reaction. *Chem. Eur. J.*, **2021**, *7*, 1–6.

(26)   Roehrich, B.; Sepunaru, L. Nanoimpacts at Active and Partially Active Electrodes: Insights and Limitations. *Angew. Chem. Int. Ed.*, **2020**, *59*, 19184–19192.

(27)   Defnet, P. A.; Zhang, B. Collision, Adhesion, and Oxidation of Single Ag Nanoparticles on a Polysulfide-Modified Microelectrode. *J. Am. Chem. Soc.*, **2021**, *143*, 16154–16162.

(28)   Azimzadeh Sani, M.; Pavlopoulos, N. G.; Pezzotti, S.; Serva, A.; Cignoni, P.; Linnemann, J.; Salanne, M.; Gaigeot, M.; Tschulik, K. Unexpectedly High Capacitance of the Metal Nanoparticle/Water Interface: Molecular- Level Insights into the Electrical Double Layer. *Angew. Chem. Int. Ed.*, **2021**, *61*, 2–10.

(29)   Hafez, M. E.; Ma, H.; Peng, Y. Y.; Ma, W.; Long, Y. T. Correlated Anodic-Cathodic Nanocollision Events Reveal Redox Behaviors of Single Silver Nanoparticles. *J. Phys. Chem. Lett.*, **2019**, *10*, 3276–3281.

(30)   Deng, Z.; Renault, C. Unravelling the Last Milliseconds of an Individual Graphene Nanoplatelet before Impact with a Pt Surface by Bipolar Electrochemistry. *Chem. Sci.*, **2021**, *12*, 12494–12500.

(31)   Pendergast, A. D.; Deng, Z.; Maroun, F.; Renault, C.; Dick, J. E. Revealing Dynamic Rotation of Single Graphene Nanoplatelets on Electrified Microinterfaces. *ACS Nano*, **2021**, *15*, 1250–1258.

(32)   Pendergast, A. D.; Renault, C.; Dick, J. E. Correlated Optical-Electrochemical Measurements Reveal Bidirectional Current Steps for Graphene Nanoplatelet Collisions at Ultramicroelectrodes. *Anal. Chem.*, **2021**, *93*, 2898–2906.

(33)   Lemineur, J. F.; Noël, J. M.; Combellas, C.; Kanoufi, F. Revealing the Sub-50 Ms Electrochemical Conversion of Silver Halide Nanocolloids by Stochastic Electrochemistry

and Optical Microscopy. *Nanoscale*, **2020**, *12*, 15128–15136.

(34) *Scanning Electrochemical Microscopy 2ⁿᵈ Edition*; Bard, A. J., Mirkin, M. V., Eds.; CRC Press, Boca Raton, **2012**.

(35) Miranda Vieira, M.; Lemineur, J. F.; Médard, J.; Combellas, C.; Kanoufi, F.; Noël, J. M. Operando Analysis of the Electrosynthesis of Ag2O Nanocubes by Scanning Electrochemical Microscopy. *Electrochem. Commun.*, **2021**, *124*, 106950.

(36) McKelvey, K.; Robinson, D. A.; Vitti, N. J.; Edwards, M. A.; White, H. S. Single Ag Nanoparticle Collisions within a Dual-Electrode Micro-Gap Cell. *Farad. Disc.*, **2018**, *210*, 189–200.

(37) Izzi, M.; Sportelli, M. C.; Ditaranto, N.; Picca, R. A.; Innocenti, M.; Sabbatini, L.; Cioffi, N. Pros and Cons of Sacrificial Anode Electrolysis for the Preparation of Transition Metal Colloids: A Review. *ChemElectroChem*, **2020**, *7*, 386–394.

(38) Trafela, Š.; Zavašnik, J.; Šturm, S.; Rožman, K. Ž. Formation of a Ni(OH)2/NiOOH Active Redox Couple on Nickel Nanowires for Formaldehyde Detection in Alkaline Media. *Electrochim. Acta*, **2019**, *309*, 346–353.

(39) Godwin, I. J.; Lyons, M. E. G. Enhanced Oxygen Evolution at Hydrous Nickel Oxide Electrodes via Electrochemical Ageing in Alkaline Solution. *Electrochem. Commun.*, **2013**, *32*, 39–42.

(40) Kim, H. S.; Itoh, T.; Nishizawa, M.; Mohamedi, M.; Umeda, M.; Uchida, I. Microvoltammetric Study of Electrochemical Properties of a Single Spherical Nickel Hydroxide Particle. *Int. J. Hydrog. Energy*, **2002**, *27*, 295–300.

(41) Clausmeyer, J.; Masa, J.; Ventosa, E.; Öhl, D.; Schuhmann, W. Nanoelectrodes Reveal the Electrochemistry of Single Nickelhydroxide Nanoparticles. *Chem. Commun.*, **2016**, *52*, 2408–2411.

(42) Ferreira, E. B.; Jerkiewicz, G. On the Electrochemical Reduction of β-Ni(OH)2 to Metallic Nickel. *Electrocatalysis*, **2021**, *12*, 199–209.

(43)   Brasiliense, V.; Noël, J.-M.; Wonner, K.; Tschulik, K.; Combellas, C.; Kanoufi, F. Single Nanoparticle Growth from Nanoparticle Tracking Analysis: From Monte Carlo Simulations to Nanoparticle Electrogeneration. *ChemElectroChem*, **2018**, *5*, 3036–3043.

(44)   Cheng, W.; Compton, R. G. Electrochemical Detection of Nanoparticles by "nano-Impact" Methods. *TrAC*, **2014**, *58*, 79–89.

(45)   Oja, S. M.; Robinson, D. A.; Vitti, N. J.; Edwards, M. A.; Liu, Y.; White, H. S.; Zhang, B. Observation of Multipeak Collision Behavior during the Electro-Oxidation of Single Ag Nanoparticles. *J. Am. Chem. Soc.*, 2017, 708–718.

(46)   Robinson, D. A.; Edwards, M. A.; Liu, Y.; Ren, H.; White, H. S. Effect of Viscosity on the Collision Dynamics and Oxidation of Individual Ag Nanoparticles. *J. Phys. Chem. C*, **2020**, *124*, 9068–9076.

(47)   Ma, W.; Ma, H.; Chen, J. F.; Peng, Y. Y.; Yang, Z. Y.; Wang, H. F.; Ying, Y. L.; Tian, H.; Long, Y. T. Tracking Motion Trajectories of Individual Nanoparticles Using Time-Resolved Current Traces. *Chem. Sci.*, **2017**, *8* (3), 1854–1861.

(48)   Ustarroz, J.; Kang, M.; Bullions, E.; Unwin, P. R. Impact and Oxidation of Single Silver Nanoparticles at Electrode Surfaces: One Shot versus Multiple Events. *Chem. Sci.*, **2017**, *8*, 1841–1853.

(49)   Ly, L. S. Y.; Batchelor-Mcauley, C.; Tschulik, K.; Kätelhön, E.; Compton, R. G. A Critical Evaluation of the Interpretation of Electrocatalytic Nanoimpacts. *J. Phys. Chem. C*, **2014**, *118*, 17756–17763.

(50)   Zhang, F.; Defnet, P. A.; Fan, Y.; Hao, R.; Zhang, B. Transient Electrocatalytic Water Oxidation in Single-Nanoparticle Collision. *J. Phys. Chem. C*, **2018**, *122*, 6447–6455.

(51)   Wehrens-Dijksma, M.; Notten, P. H. L. Electrochemical Quartz Microbalance Characterization of Ni(OH)2-Based Thin Film Electrodes. *Electrochimica Acta* **2006**, *51*, 3609–3621.

(52)   Kätelhön, E.; Tanner, E. E. L.; Batchelor-Mcauley, C.; Compton, R. G. Destructive Nano-

Impacts: What Information Can Be Extracted from Spike Shapes? *Electrochimica Acta* **2016**, *199*, 297–304.

(53) Motupally, S.; Streinz, C. C.; Weidner, J. W. Proton Diffusion in Nickel Hydroxide Films: Measurement of the Diffusion Coefficient as a Function of State of Charge. *Journal of The Electrochemical Society* **1995**, *142*, 1401–1408.